EDGE ARTICLE

Check for updates

All publication charges for this article have been paid for by the Royal Society of Chemistry

A unique trimeric triphenylene radical cation: stacking aggregation, bonding, and stability†

Rameswar Bhattacharjee, [ID] [a] Megan E. McCormack, [b] Zheng Zhou, [ID] [bc] Zheng Wei, [ID] [b] Marina A. Petrukhina [ID] *[b] and Miklos Kertesz [ID] *[a]

A new and unique π-stacking triphenylene trimer cation radical unit appears in the crystal structure of a newly synthesized salt with an oligomeric gallium(III) chloride, $[(C_{18}H_{12})_3]^{\cdot+}(Ga_3Cl_{10})^-$, which is the first triphenylene aggregate observed. The structure is attributed to a shared electron distributed over the trimer displaying π-stacking pancake bonding. Computational modeling rationalizes the appearance of a "chain-shaped" rather than a "star-shaped" gallium chloride anion as well as the reasons why the trimer, rather than a radical cation aggregate of different size, is preferred in this system. Moreover, the calculations allowed evaluation of larger cationic triphenylene radical π-stacked aggregates. Additional stabilization due to the shared single unpaired electron is calculated to remain significant at 5–7 kcal mol^{-1} for aggregates as large as 5–6 units.

1. Introduction

The aggregation of π-conjugated molecules in a parallel face-to-face π-stacking configuration is at the basis of many of their important functions including transport of electrons and spins,[1–4] excitons,[5] and their chemical reactivity in supramolecular chemistry.[6] A particularly interesting subclass contains units that can be formally identified as radicals,[7] with the radical electrons delocalized over more than one π-conjugated molecule.[3,8–11] A variety of aggregate sizes occur in these systems, from dimers ($n = 2$) to trimers ($n = 3$), to infinite π-stacked chains.[1–3,12] However, the preference for certain aggregate sizes, as well as their electronic structures and bonding, still remains poorly understood. Aggregation into a stacking configuration is most commonly attributed to van der Waals interactions (here we use the term to include dispersion, electrostatics, and steric repulsion interactions), resulting in familiar atom-over-bond or atom-over-ring configurations, as often illustrated by the stacking of base pairs in DNA.[13] A less common type displays atom-over-atom maximally overlapping π-stacking with short direct intermolecular contacts.[14] This configuration provides an effective overlap that dominates certain physical properties, such as electron and spin transport. Such intermolecular interactions have been recognized as an electron-sharing multicenter covalent-like bond, a "pancake bond" for short, connecting these π-conjugated molecules, where the intermolecular distances are shorter than the respective vdW contact distances.[15] This intermolecular electron sharing is a consequence of the unpaired electrons contained in the delocalized π-system in contrast to closed shells, which interact *via* weak vdW interactions only. The multicenter electron sharing is often described by an intermolecular formal bond order (FBO). For the discussions in this work, this is defined as:

$$\begin{aligned} \text{FBO} = &\ \text{no. of intermol. bonding electron pairs} \\ &- \text{no. of intermol. antibonding electron pairs} \end{aligned} \quad (1)$$

For example, using the classic example of the phenalenyl radical dimer, FBO = 1 (Fig. 1a; see the ESI† for BO calculations). There are more complex situations of pancake bonding, where the atom-over-atom overlap is not perfect because the maximum overlap is not possible due to lower symmetry and other factors such as side groups and crystal packing. Many highly conducting organic crystals are charge transfer salts that contain pancake bonding between well overlapping π-conjugated molecules with an FBO that is less than 1.0. Another class of highly conducting organics, Haddon's spiro-PLY materials,[3] have an FBO = 0.5. It adds to the interest in pancake bonding, that cases with double (FBO = 2)[18] and even triple (FBO = 3)[19] pancake bonds are mentioned in the literature. The majority of pancake bonded dimers and other pancake-bonded aggregates occur in charged and not in neutral radicals.[2,3,12]

[a]Department of Chemistry and Institute of Soft Matter, Georgetown University, 37th and O Streets, NW, Washington, DC 20057-1227, USA. E-mail: kertesz@georgetown.edu

[b]Department of Chemistry, University at Albany, State University of New York, 1400 Washington Avenue, Albany, NY 12222, USA. E-mail: mpetrukhina@albany.edu

[c]School of Materials Science and Engineering, Tongji University, 4800 Cao'an Road, Shanghai 201804, China

† Electronic supplementary information (ESI) available: Synthetic procedure, UV-vis spectra, powder X-ray diffraction and X-ray crystallographic data, and computational details. CCDC 2361118. For ESI and crystallographic data in CIF or other electronic format see DOI: https://doi.org/10.1039/d4sc03774j
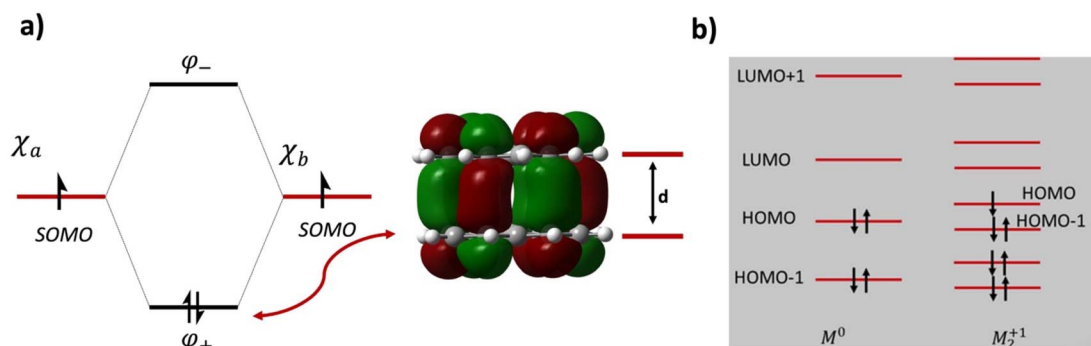
Fig. 1 (a) Molecular orbital diagram and the intermolecular bonding orbital of the prototypical phenalenyl (PLY) dimer with an intermolecular formal bond order of FBO = 1. d is the equilibrium π-stacking bond distance. The intermolecular bonding electron pair originates from the electrons in the singly occupied molecular orbitals (SOMOs) of the PLY radicals. (b) Molecular orbital diagram of a generic M_2^{1+} dimer with an intermolecular formal bond order of FBO = 0.5. Note that the HOMO of the dimer is antibonding in the intermolecular sense and it is the HOMO−1 that provides the driving force for pancake bonding. This figure is partially adapted from ref. 15–17.

Using a combination of crystallographic and theoretical tools, we recently revealed the importance of pancake bonding and cation–anion interactions in stabilizing pyrene and perylene radical dimers.[8,17,20] Although a wealth of research has been done on TCNQ and other conjugated π-stacking materials,[1–4] investigations of polycyclic aromatic hydrocarbons (PAHs) with different symmetries and sizes still remain limited. Even considering such a typical small PAH as triphenylene (TP, $C_{18}H_{12}$), where the formation of the TP cation has been previously documented, we found a lack of crystallographic structural evidence in the literature. The first detection of a cationic radical of triphenylene was made in 1965, using *in situ* electron paramagnetic resonance (EPR) during chemical oxidation.[21] Later, in 1988, another EPR study in solution further confirmed the formation of the radical cations, also achieved by chemical oxidation.[22] Moreover, in 1980, electrochemical oxidation led to the formation of two conducting solids, $[(C_{18}H_{12})_x]^{\bullet+}(PF_6^-)$ and $[(C_{18}H_{12})_x]^{\bullet+}(AsF_6^-)$, with ESR signals supporting the existence of radical species with unknown stoichiometry.[23] Besides direct oxidation, the triphenylene radical cation has also been identified through hydrogen-atom abstraction and ionization,[24,25] but, to the best of our knowledge, no crystal structures have been reported for the oxidized TP products.

After demonstrating the effect of alkali metal counterions on magnetic interactions between the triphenylene anion radicals in crystalline solids,[26] we set out to explore triphenylene oxidation in this work. Using a chemical reaction of triphenylene with GaCl₃, we isolated a unique product and confirmed its composition as $[(C_{18}H_{12})_3]^{\bullet+}(Ga_3Cl_{10})^-$ through X-ray diffraction analysis. This first triphenylene trimer radical cation was then used for advancing our understanding of bonding, the stability of π-stacking and the preference for certain aggregate sizes with the help of theoretical tools. Using well-established and validated versions of density functional theory (see the ESI† for more details), we considered periodic boundary computations on the crystal and molecular orbital computations on isolated molecules and π-stacked aggregates. In order to get deeper insights, we considered a number of factors, namely charge and spin distributions within the stacks and in the crystal, binding energies, structural features and their relationships with the relevant frontier orbitals, reduction and oxidation potentials, and preferred configurations of both cations and anions.

2. Results and discussion

2.1. Preparation and characterization of $[(C_{18}H_{12})_3]^{\bullet+}(Ga_3Cl_{10})^-$

In this work, we investigated the chemical oxidation of triphenylene (TP) with GaCl₃ in anhydrous fluorobenzene. Mixing these reagents in a 1 : 1.5 ratio at room temperature afforded a bright pink solution within two minutes. Subsequent slow evaporation of this solution over two weeks at 40 °C produced dark purple blocks suitable for X-ray diffraction analysis (see the ESI† for more details). X-ray diffraction analysis confirmed that crystals conform to a monoclinic $P2_1$ ($Z = 2$) space group with a volume of 2507.1(4) Å³ and revealed the product composition as $[(C_{18}H_{12})_3]^{\bullet+}(Ga_3Cl_{10})^-$ with no solvent incorporation. In the crystal structure, there are three crystallographically independent TP molecules with an overall positive charge for each $Ga_3Cl_{10}^-$ anion (Fig. 2a and b).

In the solid state, three TPs (designated as A, B, and C) are π-stacked with short interplanar distances ranging over 3.293(5)–3.371(5) Å in a face-to-face arrangement with high surface overlap. Within the TP stacks, the middle molecule is related to the top and bottom neighbors *via* inversion symmetry operations through two local inversion centers (Fig. S4†). The neighboring TP stacks are nearly perpendicular to each other (89.88°) and exhibit weak C–H⋯π interactions (2.871(5)–2.899(5) Å) to form a 2D network (Fig. 2d).

Each triphenylene in the trimer exhibits different H⋯Cl bonding interactions with the anionic moiety (Fig. S6†). Specifically, triphenylene C shows more H⋯Cl contacts with the $Ga_3Cl_{10}^-$ anion in comparison with A and B. Despite this, the central triphenylene B experienced the most significant core deformation, as evidenced by C–C bond length distances (Table S2†). Some bonds, such as c, e, and k, exhibit more notable contraction (0.041 Å, 0.034 Å, and 0.035 Å, respectively), while bonds i, j, and l show significant elongation (0.071 Å, 0.072 Å,
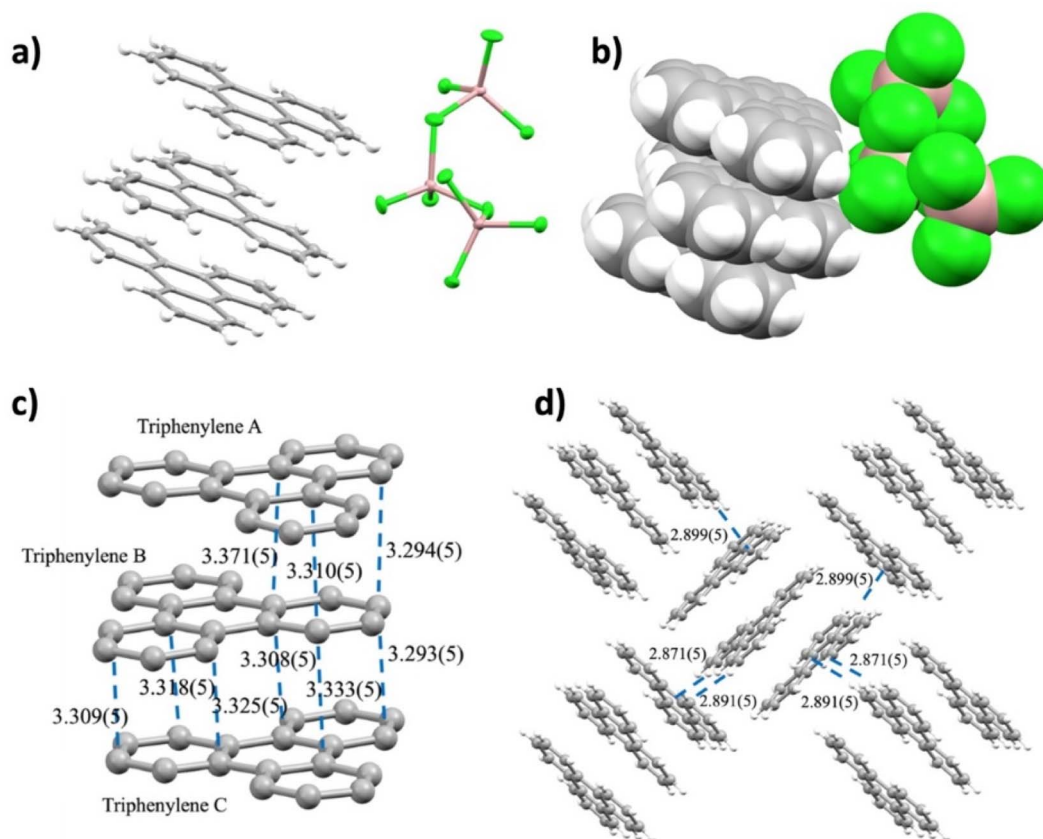
Fig. 2 (a) ORTEP drawing of $[(C_{18}H_{12})_3]^{\bullet+}(Ga_3Cl_{10})^-$ with thermal ellipsoids shown at the 50% probability level. (b) Space-filling model of $[(C_{18}H_{12})_3]^{\bullet+}(Ga_3Cl_{10})^-$. (c) Interplanar distances within the triphenylene π-stacked trimer, and H atoms are omitted for clarity. (d) Illustration of C–H···π contacts in the 2D network of $[(C_{18}H_{12})_3]^{\bullet+}(Ga_3Cl_{10})^-$.

and 0.033 Å, respectively). However, triphenylene A demonstrates the most significant deviation in dihedral angles, suggesting a slight loss of planarity compared to neutral triphenylene (Table S3†).

Interestingly, the gallium(III) chloride anion, $Ga_3Cl_{10}^-$, in this charge transfer salt exhibits a "chain-shaped"[27] rather than a "star-shaped" configuration.[28] The preference of the former over the latter is discussed and rationalized below in the theory section.

In addition to single crystal X-ray diffraction, further product characterization was performed through electron paramagnetic resonance (EPR) spectroscopy (Fig. 3), UV-vis spectroscopy (Fig. S7†), powder X-ray diffraction (Fig. S8†), and ATR-IR spectroscopy (Fig. S9†). The EPR spectra were collected on the crystalline samples of $[(C_{18}H_{12})_3]^{\bullet+}(Ga_3Cl_{10})^-$ (Fig. 3), showing a g-factor of 2.0031 and confirming the presence of organic-based radicals in the product (see the ESI† for the details). The presence of unpaired electrons is essential for understanding the special aggregation mechanism via pancake bonding, as discussed in the next section.

2.2. Computational investigation

Pancake bonding plays a central role in unraveling the structural features and preferences to be discussed next. The consequence of pancake bonding is an atom-over-atom
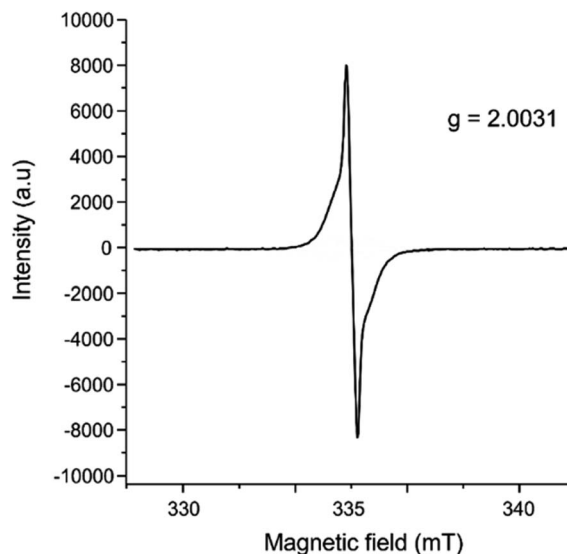

Fig. 3 EPR spectrum of crystalline $[(C_{18}H_{12})_3]^{\bullet+}(Ga_3Cl_{10})^-$, collected at 31.9 °C on a LINEV ADANI Spinscan X Electron Paramagnetic Resonance Spectrometer.

geometry and a shorter than vdW packing with a partial covalent character. Two measures of interaction energies, the total interaction energy ($\Delta E_{\text{int},n}^q$, eqn (S1) in the ESI†) and the average

interaction energy per pair ($\Delta E_{pair}{}^q$, eqn (S2) in the ESI†), are discussed. In addition, the charge distribution among the different TP units provides further insights, which is the starting point of the computational analysis. Fig. 4a illustrates the unit cell of the crystal structure of $[(C_{18}H_{12})_3]^{\cdot+}(Ga_3Cl_{10})^-$, containing two formula units and consisting of six TP units organized into two isolated trimers, each carrying a +1 charge. The crystal's charge neutrality is achieved through the inclusion of two "chain-shaped" $Ga_3Cl_{10}^-$ counterions within the unit cell. The charge analysis indicates that the $q = +2$ charge is distributed among the two TP trimers, each carrying a $Q = +1$ charge. This charge is unevenly distributed within one trimer across three TP units. Specifically, the central triphenylene (TP-B/TP-B′) holds the most significant positive charge of +0.47, while the charges on the terminal units (TP-A/TP-A′ and TP-C/TP-C′) are +0.21 and +0.19, respectively. Note that the small difference between the two terminal charges is due to the lack of symmetry in the crystal structure, in contrast to the charge distribution in the isolated trimer, as discussed below. Fig. 4b presents the computed charges for each TP within the unit cell.

Correspondingly, the spin density plot shown in Fig. 4c corroborates the Bader charge analysis, indicating that the middle TP unit possesses the highest spin density, and thus the greatest positive charge, compared to the two terminal units. Additionally, analysis of the HOMO−1 of the unit cell reveals significant intermolecular orbital overlap, indicating the presence of pancake bonding within the trimer. We focused on the HOMO−1 because it plays a crucial role in the properties of a +1-charged perylene dimer in our earlier studies.[17,20]

The crystal structure underscored the distinct formation of a trimeric TP aggregate, prompting a thorough exploration of its bonding and underlying formation mechanism. To this end, we evaluated the free energy (ΔG) required for a one-electron reduction of the chain-shaped $Ga_3Cl_{10}^-$, which was found to be −166.2 kcal mol⁻¹. This energy threshold sets the limit for oxidizing species with an oxidation free energy that is lower than this value. Fig. 5a presents the calculated free energies of oxidation for triphenylene in its monomeric, dimeric, and trimeric forms. Specifically, the oxidation of the monomer $[(C_{18}H_{12})]$ and the dimer $[(C_{18}H_{12})_2]$ would require 179.1 kcal
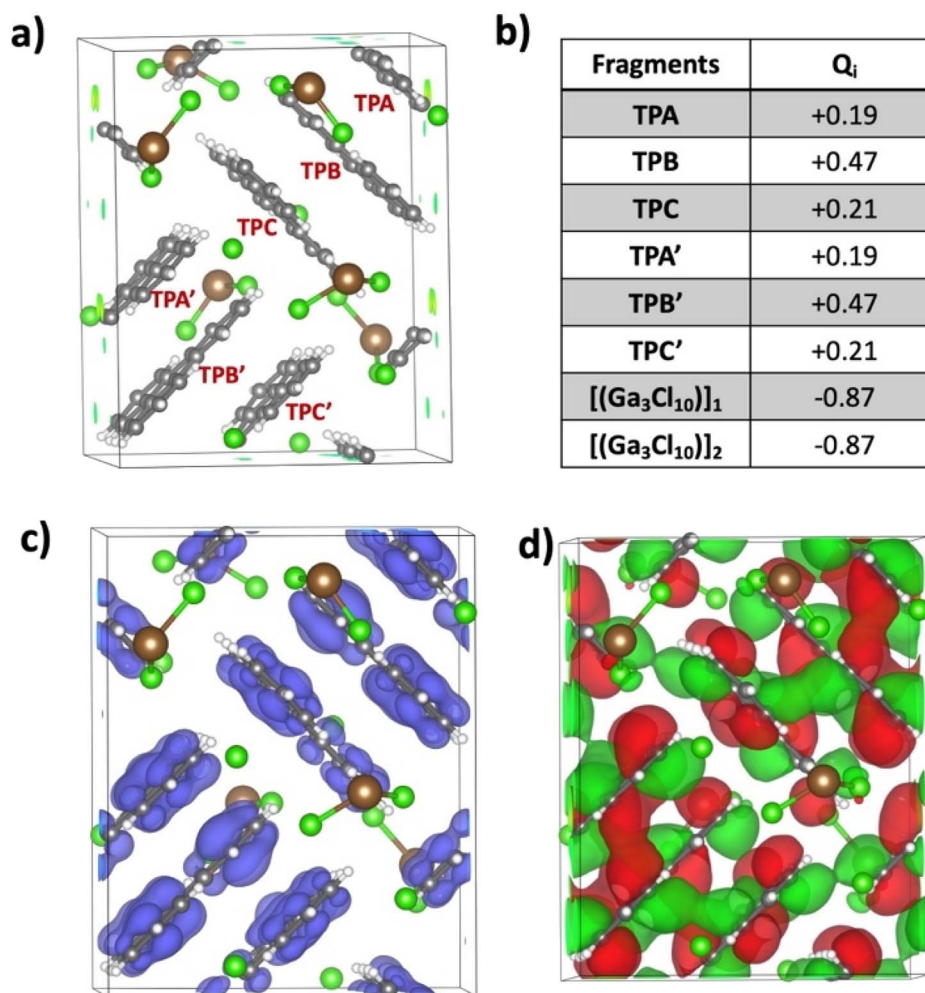

Fragments	Q_i
TPA	+0.19
TPB	+0.47
TPC	+0.21
TPA′	+0.19
TPB′	+0.47
TPC′	+0.21
$[(Ga_3Cl_{10})]_1$	-0.87
$[(Ga_3Cl_{10})]_2$	-0.87

Fig. 4   (a) Unit cell of the crystal structure $[(C_{18}H_{12})_3]^{\cdot+}(Ga_3Cl_{10})^-$ ($Z = 2$), comprising six triphenylene units and two $Ga_3Cl_{10}^-$ anions. (b) Fractional charge values (Q_i) are computed for each of the TP molecules and Ga(III) chloride counter anions in the unit cell. (c) Spin density distribution in the unit cell (|iso| = 0.0003). (d) The HOMO−1, illustrating intermolecular overlap (|iso| = 0.00005).

a) Reduction

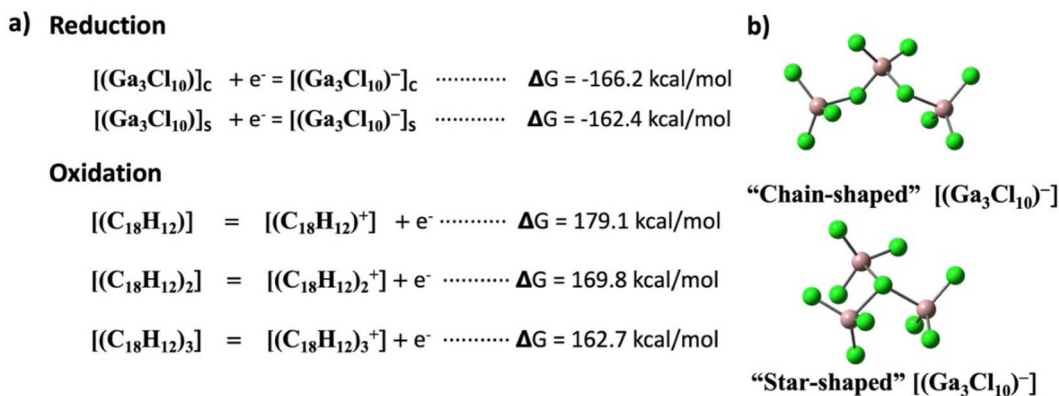$$[(Ga_3Cl_{10})]_C + e^- = [(Ga_3Cl_{10})^-]_C \quad \cdots\cdots \quad \Delta G = -166.2 \text{ kcal/mol}$$

$$[(Ga_3Cl_{10})]_S + e^- = [(Ga_3Cl_{10})^-]_S \quad \cdots\cdots \quad \Delta G = -162.4 \text{ kcal/mol}$$

Oxidation

$$[(C_{18}H_{12})] = [(C_{18}H_{12})^+] + e^- \quad \cdots\cdots \quad \Delta G = 179.1 \text{ kcal/mol}$$

$$[(C_{18}H_{12})_2] = [(C_{18}H_{12})_2^+] + e^- \quad \cdots\cdots \quad \Delta G = 169.8 \text{ kcal/mol}$$

$$[(C_{18}H_{12})_3] = [(C_{18}H_{12})_3^+] + e^- \quad \cdots\cdots \quad \Delta G = 162.7 \text{ kcal/mol}$$

b)

"Chain-shaped" $[(Ga_3Cl_{10})^-]$

"Star-shaped" $[(Ga_3Cl_{10})^-]$

Fig. 5 (a) Computed free energy values for the formation of chain- and star-shaped $Ga_3Cl_{10}^-$ through one-electron reduction. ΔG for one-electron oxidation of TP monomers, dimers, and trimers. "C" and "S" subscripts in the formula stand for "chain-shaped" and "star-shaped", respectively. (b) Optimized molecular structures of chain-shaped and star-shaped $Ga_3Cl_{10}^-$.

mol^{-1} and 169.8 kcal mol^{-1} respectively, making oxidation by the chain-shaped $Ga_3Cl_{10}^-$ anion not viable due to the resulting positive, non-spontaneous reaction free energies. However, the situation differs for the trimer $[(C_{18}H_{12})_3]$, where the oxidation energy is 162.7 kcal mol^{-1}, 3.5 kcal mol^{-1} less than the reduction free energy of the $Ga_3Cl_{10}^-$ chain. This permits the oxidation of the trimer by the chain-shaped $Ga_3Cl_{10}^-$, rendering the overall reaction and the formation of $[(C_{18}H_{12})_3]^{\cdot+}(Ga_3Cl_{10})^-$ energetically favorable and exergonic by 3.5 kcal mol^{-1}.

A star-shaped isomer of $Ga_3Cl_{10}^-$ has been described in the literature.[27,28] Why is the chain structure favored in the title crystal structure over the "star-shaped" one? According to the computational modeling presented in Fig. 5a, the reduction is strongly preferred by the chain-shaped $Ga_3Cl_{10}^-$, which is indeed the observed configuration in the crystal. Further details on both types of $Ga_3Cl_{10}^-$ are provided in the ESI (see Scheme S2†). It is crucial to recognize that while Madelung (electrostatic, Coulomb) energy significantly contributes to the stability of an ionic crystal, it predominates only after the crystal forms and the ions are appropriately arranged in the crystal phase. This analysis not only justifies our use of the chain variant of $Ga_3Cl_{10}^-$ but also elucidates why the trimeric TP cluster preferentially forms under the experimental conditions.

In the following, we address the nature of intermolecular electron sharing by discussing the computational modeling of different-size TP aggregates all with $q = +1$ charge (see eqn S(3)†). We begin with the $n = 3$, $[(C_{18}H_{12})_3]^+$, trimer, followed by other π-stacked aggregates. This investigation primarily focused on delineating the strength of the interactions among TPs within the trimer and other aggregates. The total interaction energy among the triphenylene units in the trimer is computed to be -44.1 kcal mol^{-1}. This is a relatively high interaction energy compared to the typical van der Waals interaction energy and we show that it is due to pancake bonding (PCB).[29] PCB is distinguished by its robust, directionally specific nature, arising from atom-over-atom overlaps, which play a pivotal role in stabilizing radical-containing PAH systems.[11,15,17,30] In the optimized trimer, 24 short C$\cdots$C contacts were identified with an average interplanar distance (d_{av}, see

eqn (3) in the ESI†) of 3.29 Å, noticeably below the van der Waals contact distance of 3.40 Å, another feature of pancake bonding. Both the top and side views of the optimized structures of $[(C_{18}H_{12})_3]^+$ are depicted in Fig. 6a and b, respectively. Charge distribution within the trimer revealed an uneven yet symmetric charge distribution: the central TP possesses a charge of +0.62e, with each terminal TP unit carrying +0.19e. This pattern aligns with the Bader charge distribution previously computed for the unit cell. To further validate this uneven charge distribution in the trimer, additional popular charge analyses—NPA,[31] Mulliken, and Hirshfeld[32]—were conducted, with the results summarized in Table S5.† Additionally, the spin density plot, shown in Fig. 6c, also supports the observation of the uneven charge distribution across the trimer.

Orbital analysis further reveals that the SOMO of the trimer exhibits antibonding characteristics, and three occupied orbitals demonstrate significant intermolecular bonding interactions, as illustrated in Fig. 6e, indicating the characteristic pancake bonding within the trimer.

Although the trimeric aggregate was the focus of our experimental observations, altering experimental conditions in the $[(C_{18}H_{12})_n]^+$ series may potentially enable the isolation of other types as well. Understanding the nature of interactions among TP molecules within these aggregates is crucial for exploring their properties and potential applications. The simplest aggregate, the dimer, is next, followed by larger aggregates. In all cases $q = +1$ overall charge is assumed. We follow how the unpaired electron generates a variety of pancake-bonded structures, and how this effect diminishes as n is increased up to $n = 6$.

The average interplanar distance (d_{av}) in the $[(C_{18}H_{12})_2]^+$ dimer is computed to be 3.26 Å, suggesting the involvement of interactions beyond van der Waals forces. As depicted in Fig. 7a, twelve C$\cdots$C short contacts ranging from 3.23 Å to 3.30 Å were identified. Orbital analysis revealed the antibonding nature of the SOMO and a series of occupied orbitals demonstrating bonding (in-phase) intermolecular orbital overlap, confirming the presence of pancake bonding (PCB), as depicted in the MO diagram in Fig. 7c. An FBO value of 1/2 can be deduced from
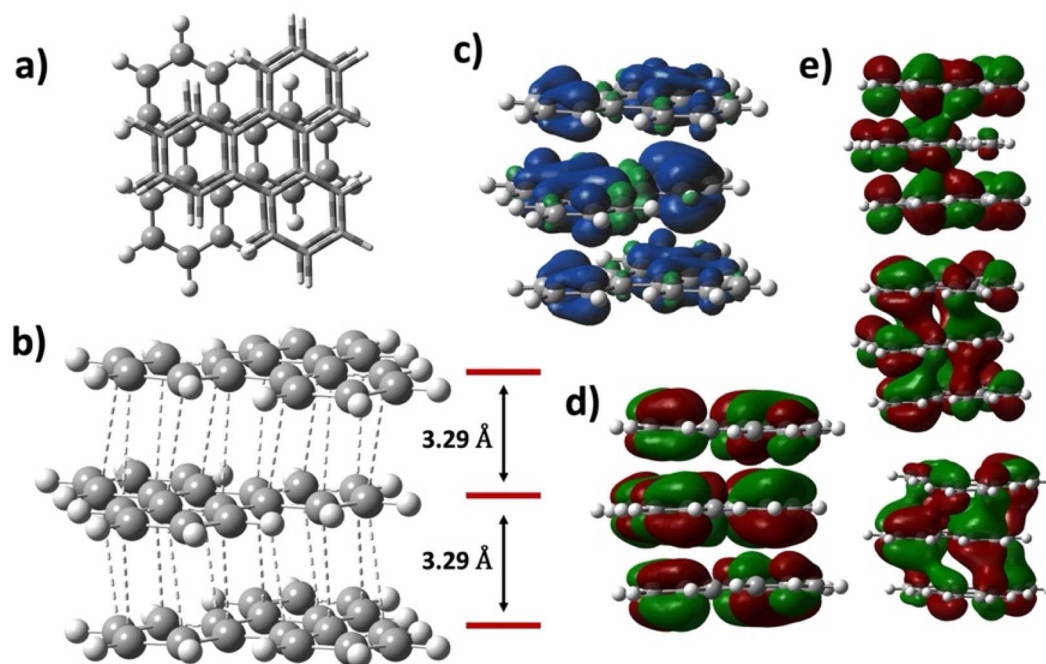
Fig. 6 (a) Top view of the optimized structure of the trimer, $[(C_{18}H_{12})_3]^+$. (b) Side view of the optimized structure of $[(C_{18}H_{12})_3]^+$, showcasing C···C short contacts represented by dashed lines; (c) spin density distribution ($|iso| = 0.0008$). (d) SOMO (Singly Occupied Molecular Orbital) of the trimer. (e) Three occupied orbitals displaying intermolecular $\pi-\pi$ overlap showing the characteristics of the pancake bond (PCB). Orbitals are plotted using $|iso| = 0.015$.

this MO diagram. The interaction energy between TP molecules in the dimer is calculated to be -24.6 kcal mol^{-1}, significantly larger than typical van der Waals values. In comparison, we note that the experimentally determined binding energy in the benzene cation dimer is $\Delta H = 17.6$ kcal mol^{-1},[33] significantly larger than the vdW binding energy. Moreover, the equal charge distribution of the $q = +1$ charge ($+0.5$ e on each TP) and consistent symmetrical spin density distribution (Fig. 7b)
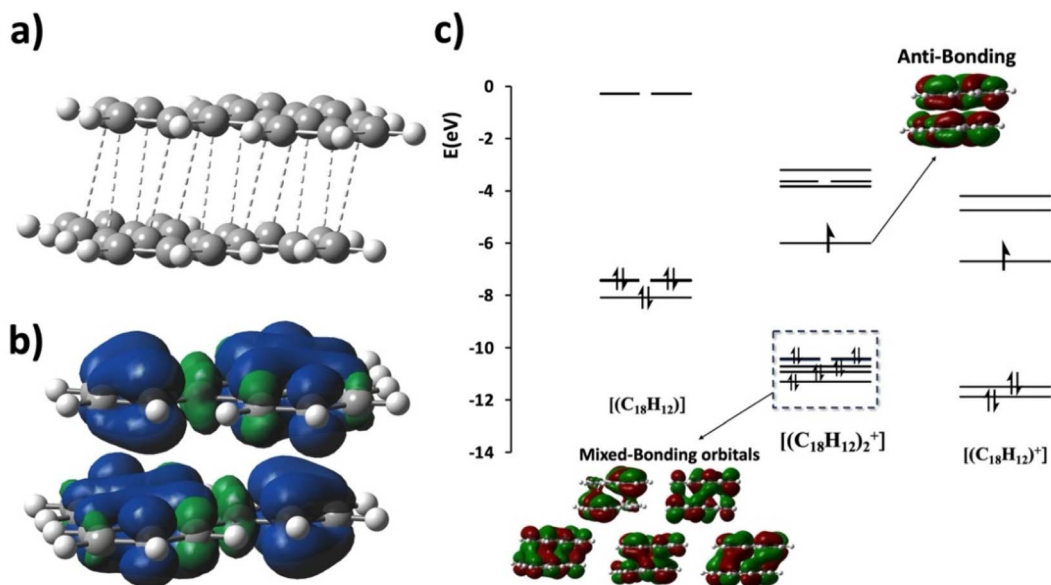

Fig. 7 (a) Optimized structure of the mono-cationic TP dimer, $[(C_{18}H_{12})_2]^+$, with dashed lines highlighting short C···C contacts. (b) Spin density of $[(C_{18}H_{12})_2]^+$. (c) Molecular orbital (MO) diagram for $[(C_{18}H_{12})_2]^+$, showing ten valence orbitals derived from the combination of five valence orbitals each from the neutral and cationic triphenylene monomers. Spin density is plotted using $|iso| = 0.0008$ and orbitals are plotted using $|iso| = 0.015$.

across the dimer underscore the delocalization of the unpaired electron and validate the interpretation of this bonding as a PCB interaction. We note parenthetically that employing the same DFT and basis set of (U)M05-2X/6-311G(d), we obtained $\Delta H_{binding} = 18.9$ kcal mol^{-1} for $[(C_6H_6)_2]^+$, which is in very good agreement with the experimental value[33] of 17.6 kcal mol^{-1}, in line with our earlier validation study providing strong support to use this level of theory for pancake bonding of PAHs.[34]

We analyze the pancake bonding in the $[(C_{18}H_{12})_n]^+$ aggregate series in terms of the intermolecular packing and charge distribution first, and then turn to the interaction energies. Fig. 8 summarizes how the additional $q = +1$ charge is delocalized over the constituent TPs and shows the average interplanar distances (d_{av}). The respective FBO value remains 1/2 as per eqn (1), although this bond order is distributed among $n - 1$ intermolecular contacts. As noted earlier, in the dimer, each triphenylene uniformly carries the total +1 charge, while in the trimer, an uneven but symmetrical charge distribution is evident. In the tetramer, the charge distribution remains symmetrical but unequal: the two central TP units bear +0.40e charge each, and the terminal molecules each have +0.10e. Our observations indicate that the charges on the terminal TPs diminish as the column length increases, disappearing almost entirely beyond n

$= 4$. As shown in the last two images for $n = 5$ and 6, the charge distribution among the central TP units remains symmetrical, and the two terminal TP units are neutral. Thus, the influence of the +1 charge does not extend significantly beyond $n = 4$.

The average interplanar distances (d_{av}) also show an interesting pattern. For the dimer and trimer, the values are significantly below the vdW distance of 3.4 Å in concordance with PCBs. The picture changes for $n > 3$. Already at $n = 4$ only the central d_{av} remains significantly below 3.4 Å, while the two terminal d_{av} values approach 3.4 Å. This trend continues as n increases, and for $n = 6$ the terminal d_{av} values are nearly 3.4 Å. At the same time, the central d_{av} values also decrease. These trends suggest that for larger n the two terminal TPs are attached to the rest of the aggregate by an interaction not very different from ordinary vdW, without the assistance of PCB. At the same time, the single unpaired electron that is available for PCB is being diluted, and all d_{av} values gradually approach the vdW value. Is the analysis of the energetics showing the same trends?

The computational method section describes the approach for calculating the total interaction energy ($\Delta E_{int,n}^q$) between triphenylene molecules in stacked columns, as shown in eqn (S1) in the ESI.† Those interaction energies for both mono-
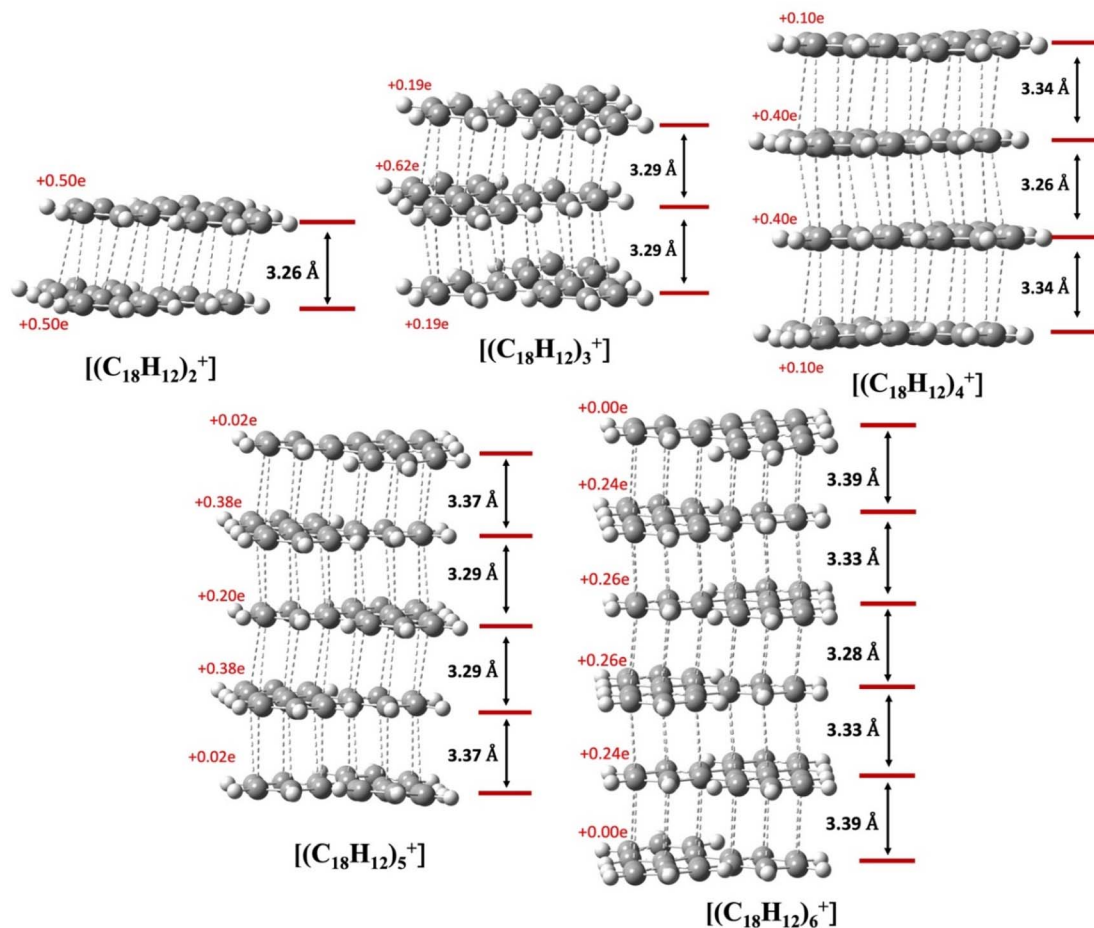

Fig. 8 π-Stacked columns of different sized TP cation radical aggregates, $[(C_{18}H_{12})_n]^+$, with n ranging from 2 to 6. Dashed lines indicate short C···C contacts and the red numbers on each TP represent the partial charge of that unit. The black double-headed arrows are shown for each pair of TPs to denote the inter-planar distances (d_{av}).

Table 1 Total interaction energies ($\Delta E_{\text{int},n}{}^{q}$) and average interaction energies per pair ($\Delta E_{\text{pair}}{}^{q}$) of triphenylenes in stacked columns with total charge q. For the definitions, see the ESI

TP column	$\Delta E_{\text{int},n}{}^{q=+1}$	$\Delta E_{\text{int},n}{}^{q=0}$	$\Delta E_{\text{pair}}{}^{q=+1}$	$\Delta E_{\text{pair}}{}^{q=0}$
$[(C_{18}H_{12})_2]^q$	−24.6	−12.7	−24.6	−12.7
$[(C_{18}H_{12})_3]^q$	−44.1	−24.6	−22.1	−12.3
$[(C_{18}H_{12})_4]^q$	−60.5	−36.2	−20.2	−12.1
$[(C_{18}H_{12})_5]^q$	−75.0	−47.8	−18.7	−11.9
$[(C_{18}H_{12})_6]^q$	−88.2	−59.5	−17.6	−11.9

cationic and neutral aggregates are detailed in Table 1. The interaction energy differences between the charged and neutral aggregates are denoted as $\Delta E_{\text{int},n}{}^{q=+1}$ and $\Delta E_{\text{int},n}{}^{q=0}$, respectively. This key difference highlights that the presence of a +1 charge favors the aggregation with stronger cohesion within the TP π-stacks due to pancake bonding. While the attachment of the second TP is smaller than the first (−22.1 *vs.* −24.6 kcal mol^{-1}), it is still a remarkably strong bonding interaction. A similar effect has been observed on the heteromolecular attachment of the second benzene molecule to a naphthalene +1 cation *vs.* the attachment of the first, both with essentially the same ~8 kcal mol^{-1}.[35]

The dependency of these interaction energies on the number of triphenylenes (n) in the π-stacking aggregate is illustrated in Fig. 9a. For neutral stacks, the plot of $\Delta E_{\text{int},n}{}^{q}$ versus n is perfectly linear, with an R^2 value of 1.0. In contrast, the energy relationship for stacks carrying a +1 charge displays a slightly nonlinear trend and a steeper slope for small n values. The absolute difference becomes more pronounced as n increases, likely due to a larger number of close carbon–carbon (C···C) contacts as more triphenylenes are added to the column.

To compute the average interaction energy per pair ($\Delta E_{\text{pair}}{}^{q}$) of triphenylene molecules in a π-stacked column, we introduced an extension of eqn (S1),† defined as eqn (S2) in the ESI section.† The values for $\Delta E_{\text{pair}}{}^{q}$ are also listed in Table 1, showing that the average interaction energy remains relatively constant for neutral stacks. In contrast, for mono-cationic stacks, this value decreases gradually from −24.6 kcal mol^{-1} for the dimer to −17.6 kcal mol^{-1} for the hexamer. This analysis confirms that the additional positive charge significantly influences the structural stability within the stacks.

We further explored the interaction energy, denoted as $\Delta E_n{}^{q}$, involved in sequentially adding one neutral TP ring to the complex $[(C_{18}H_{12})_{n-1}]^q$ to form $[(C_{18}H_{12})_n]^q$. This measure provides an estimate of the affinity of $[(C_{18}H_{12})_{n-1}]^q$ to incorporate another TP unit into the column. This interaction energy is calculated using the following equation:

$$\Delta E_n{}^{q} = E_{[(C_{18}H_{12})_n]^q} - E_{[(C_{18}H_{12})_{n-1}]^q} - E_{[(C_{18}H_{12})]1} \tag{2}$$

where $q = +1$ for the cationic series and $q = 0$ for the neutral series. The difference between $\Delta E_n{}^{q=+1}$ and $\Delta E_n{}^{q=0}$ estimates the contribution of PCB in the formation of $[(C_{18}H_{12})_n]^q$ from $[(C_{18}H_{12})_{n-1}]^q$. Fig. 9b displays the variation of $\Delta E_n{}^{q}$ as a function of $1/n$, showing a linear trend for the mono-cation aggregate with an R^2 value of 0.996. For the neutral system, the

dependency on n is minimal, in agreement with the fact that only vdW interactions are at work.

The higher negative value of $\Delta E_n{}^{q=+1}$ at any given $1/n$ suggests a stronger tendency for $[(C_{18}H_{12})_{n-1}]^{+1}$ to attract another TP. The steeper slope of −34.11 in the plot (depicted by a black line through red data points in Fig. 9b) indicates that the affinity for adsorbing an additional neutral TP onto the mono-cationic $[(C_{18}H_{12})_{n-1}]^{+1}$ aggregate decreases sharply as $1/n$ decreases (*cf.* Fig. S10†). This phenomenon is largely due to the presence of PCB, which is more effective when there is a higher concentration of unpaired electron density among the TPs. As the number of TPs increases, this effect diminishes since the electron density becomes more distributed. However, and this is one of the key results here, for aggregates as large as $n = 3$ or 4, there is still substantial pancake bonding present, driving the formation of the aggregates.

Several studies demonstrated the impact of fractional charges on bond length alternation (BLA),[36] a key indicator of conjugation patterns in π-electron systems.[8,17,37] This effect is also observed in triphenylene, as illustrated in Fig. S11.† In its neutral state, triphenylene exhibits a high degree of symmetry of the D_{3h} point group. However, when the charge is increased to +1, the symmetry decreases to C_s. Another structure of TP$^+$, belonging to the C_{2v} point group, is nearly energetically equivalent to the C_s form and exhibits a minimal imaginary mode frequency of 15 cm^{-1}. This symmetry reduction is primarily due to Jahn–Teller (JT) distortion, a phenomenon previously discussed in depth by Keszthelyi *et al.*[38] As a result of JT distortion, the C–C bond lengths in the +1 charged triphenylene become uneven: some bonds elongate while others shorten, as shown in Fig. S11d,† when compared to the symmetric neutral state in Fig. S11a.† The triphenylene molecule with a fractional charge (Q) of +0.5 also exhibits C_s symmetry, akin to the fully +1 charged state, but with variations in the degree of bond elongation and compression, as depicted in Fig. S11c.† The structures of the other triphenylenes with different fractional charges are also provided in Fig. S12.† It is important to note that when discussing fractional charges (Q_i), the resulting structure does not represent a true minimum of a single TP but rather is part of an aggregate.

To better understand the structural changes in triphenylene as its charge (Q) varies, we employed the harmonic oscillator model of aromaticity (HOMA),[39] a geometry-based aromaticity index, for triphenylene with various fractional charges (Fig. S12†). Triphenylene features two types of six-membered rings: one central and three peripheral rings. The central ring in triphenylene is less aromatic compared to the peripheral ones and as noted by Krygowski and Szatylowicz,[40] the lower aromaticity of the central TP ring correlates with higher bond length alternation (BLA) values. This ring is referred to as the 'empty' ring in Clar's classification system, which signifies a deficit of π-electrons.[41] However, our analysis reveals that increasing the fractional charge on triphenylene slightly enhances the aromaticity of the central ring. Conversely, the peripheral rings exhibit a decrease in aromaticity with increasing positive charge, although this effect is less pronounced.
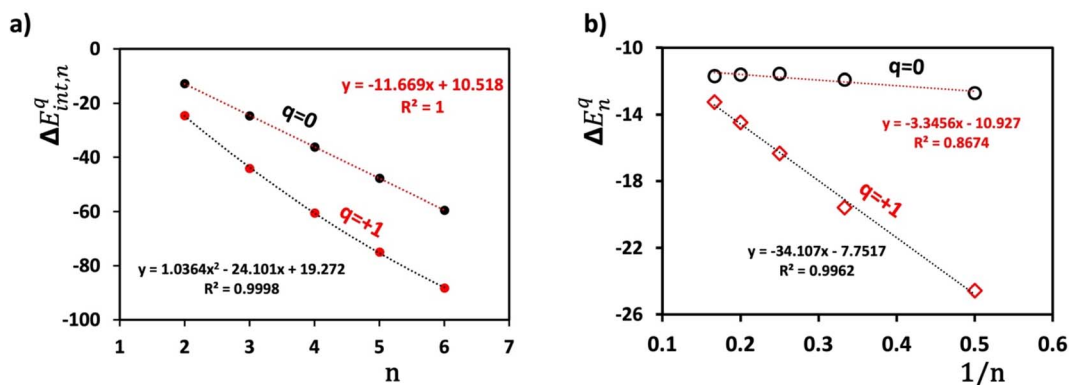
Fig. 9 (a) The variation of total interaction energy ($\Delta E_{int,n}^{q}$) as a function of the number of triphenylenes (n) in the stacked column in the $[(C_{18}H_{12})_n]^q$ series. (b) Variation in interaction energy (ΔE_n^q), eqn (1). Red marks represent the mono-cationic cluster ($q = +1$), and black marks denote the corresponding neutral cluster ($q = 0$).

3. Conclusions

In this work, we report a unique triphenylene salt, wherein chemical oxidation of triphenylene with $GaCl_3$ and subsequent crystallization confirmed the formation of $[(C_{18}H_{12})_3]^{\cdot+}(Ga_3Cl_{10})^-$ through X-ray diffraction analysis. Structural analysis revealed unusual trimers of TP units showing a face-to-face arrangement, sufficient surface overlap, and interplanar distances ranging from 3.293(5) to 3.371(5) Å. In the solid state, an extended 2D-network is formed through weak C–H$\cdots\pi$ interactions between neighboring TP trimers and H$\cdots$Cl contacts with a unique "chain-shaped" $Ga_3Cl_{10}^-$ anion. The presence of unpaired electrons is confirmed by EPR ($g = 2.0031$) and these are key to the special aggregation mechanism provided by the sharing of this unpaired electron among the trimeric TP units in pancake bonding.

According to the computational analysis, the "chain-shaped" $Ga_3Cl_{10}^-$ isomer as the counter anion is preferred over the "star-shaped" isomer. Notably, the findings suggest that the smallest energetically favorable configuration for a singly positively charged TP stack, when paired with a $Ga_3Cl_{10}^-$ chain as the counter anion, is a trimer, identified as $[(C_{18}H_{12})_3]^+$, and this aggregate is indeed the form found experimentally.

We identified pancake bonding interactions within the trimeric TP aggregate, as well as in other aggregates with varying numbers of π-stacked TP units. For comparison, the binding energy between TPs in the dimer, $[(C_{18}H_{12})_2]^+$, is calculated to be 11.9 kcal mol^{-1} higher than that of its neutral counterpart, indicating a robust pancake bonding interaction. In the trimer, this pancake bonding interaction is slightly weaker, attributed to the distribution of a single electron among three TP units, as opposed to two. As a general pattern, the strength of the pancake bonding interaction diminishes as the number of TP units in the stack increases. However, additional interaction energy due to pancake bonding remains significant even in the pentamer and the hexamer of TP. This additional interaction energy is available to stabilize larger aggregates than would be otherwise available for closed-shell neutral PAHs. This type of aggregation promoted by unpaired electrons in radicals has been proposed as a possible mechanism in the formation of naturally occurring PAH asphaltene aggregates.[42]

The preferred size of the aggregate is affected by a number of factors, and any discussion is, by necessity, only qualitative. Nevertheless, important insights and trends can be obtained. The synergy of π-stacking aggregation in the vicinity of a cation or anion has been shown to be a rather general phenomenon.[6,43] We point out in the presented work that in the context of a specific anion, the aggregation attains an optimum size due to a diminishing synergistic energy gain limiting the growth of the aggregate on the one hand, and a minimum size that ensures favorable ΔG for oxidation–reduction necessary to achieve charge transfer that allows multicenter pancake bonding to occur.

By considering π-stacked aggregates with increasing sizes, several interesting trends have been revealed. The charge distribution is uniform in the dimer but it becomes uneven yet symmetrical in larger clusters. As the size is increased, the terminal units share less and less of the additional single charge, while the rest of the charge is distributed more and more evenly over the π-stacked TP aggregate. The per unit charge therefore overall decreases with increasing size, and this dilution of the pancake bonding effect reduces the relative energy stabilization gained by each additional TP molecule. Still, the additional stabilization energy remains substantial, as large as 5–7 kcal mol^{-1} for aggregates as large as 5–6 units. It is likely that with an appropriate choice of counterion and PAH combination, a number of such aggregates will be discovered. Therefore, the new findings of this work should pave the way for future experimental discoveries in this field.

Data availability

Synthetic procedures, UV-vis and IR spectra, powder X-ray diffraction data, X-ray crystallographic data, and computational details are included in the ESI.†

Author contributions

R. B. and M. E. M. contributed equally. Z. Z. first synthesized the product, and M. E. M. optimized the synthesis, improved the crystal structure, and completed product characterization and data analysis. X-ray diffraction experiments and refinements

were performed by Z. W. R. B. carried out all calculations and wrote the first draft. M. A. P. and M. K. supervised this project and secured the funding.

Conflicts of interest

There are no conflicts to declare.

Acknowledgements

References

1 J. Ferraris, D. Cowan, V. t. Walatka and J. Perlstein, Electron transfer in a new highly conducting donor-acceptor complex, *J. Am. Chem. Soc.*, 1973, **95**(3), 948–949.

2 A. Heeger, Charge-Density Wave Phenomena in One-Dimensional Metals: TTF-TCNQ and Related Organic Conductors, in *Highly conducting one-dimensional solids*, Springer, 1979; pp. pp. 69–145.

3 S. Pal, M. Itkis, F. Tham, R. Reed, R. Oakley and R. Haddon, Resonating valence-bond ground state in a phenalenyl-based neutral radical conductor, *Science*, 2005, **309**(5732), 281–284.

4 A. Shimizu, T. Kubo, M. Uruichi, K. Yakushi, M. Nakano, D. Shiomi, K. Sato, T. Takui, Y. Hirao and K. Matsumoto, Alternating covalent bonding interactions in a one-dimensional chain of a phenalenyl-based singlet biradical molecule having Kekulé structures, *J. Am. Chem. Soc.*, 2010, **132**(41), 14421–14428.

5 X.-H. Jin, M. B. Price, J. R. Finnegan, C. E. Boott, J. M. Richter, A. Rao, S. M. Menke, R. H. Friend, G. R. Whittell and I. Manners, Long-range exciton transport in conjugated polymer nanofibers prepared by seeded growth, *Science*, 2018, **360**(6391), 897–900.

6 A.-B. Bornhof, A. Bauzá, A. Aster, M. Pupier, A. Frontera, E. Vauthey, N. Sakai and S. Matile, Synergistic Anion–$(\pi)_n$–π Catalysis on π-Stacked Foldamers, *J. Am. Chem. Soc.*, 2018, **140**(14), 4884–4892.

7 V. Enkelmann, K. Göckelmann, G. Wieners and M. Monkenbusch, Radical Cation Salts of Arenes. Structure, Properties and Model Character for Conducting Polymers, *Mol. Cryst. Liq. Cryst.*, 1985, **120**(1), 195–204.

8 C. Flynn, Z. Zhou, M. E. McCormack, Z. Wei, M. A. Petrukhina and M. Kertesz, Bonding and uneven charge distribution in infinite pyrene pi-stacks, *CrystEngComm*, 2022, **24**(32), 5757–5766, DOI: **10.1039/d2ce00933a**.

9 Z. Mou and M. Kertesz, Pancake Bond Orders of a Series of π-Stacked Triangulene Radicals, *Angew. Chem., Int. Ed.*, 2017, **56**(34), 10188–10191.

10 K. Molčanov, C. Jelsch, B. Landeros, J. Hernández-Trujillo, E. Wenger, V. Stilinović, B. Kojić-Prodić and E. C. Escudero-Adán, Partially Covalent Two-Electron/Multicentric Bonding between Semiquinone Radicals, *Cryst. Growth Des.*, 2019, **19**(1), 391–402, DOI: **10.1021/acs.cgd.8b01484**.

11 K. E. Preuss, Pancake bonds: π-stacked dimers of organic and light-atom radicals, *Polyhedron*, 2014, **79**, 1–15.

12 F. H. Herbstein and M. Kapon, Classification of closed shell TCNQ salts into structural families and comparison of diffraction and spectroscopic methods of assigning charge states to TCNQ moieties, *Crystallogr. Rev.*, 2008, **14**(1), 3–74.

13 C. R. Martinez and B. L. Iverson, Rethinking the term "pi-stacking", *Chem. Sci.*, 2012, **3**(7), 2191–2201.

14 T. Devic, M. Yuan, J. Adams, D. C. Fredrickson, S. Lee and D. Venkataraman, The maximin principle of π-radical packings, *J. Am. Chem. Soc.*, 2005, **127**(42), 14616–14627.

15 M. Kertesz, Pancake bonding: An unusual Pi-stacking interaction, *Chem.–Eur. J.*, 2019, **25**(2), 400–416.

16 Z.-h. Cui, A. Gupta, H. Lischka and M. Kertesz, Concave or convex π-dimers: the role of the pancake bond in substituted phenalenyl radical dimers, *Phys. Chem. Chem. Phys.*, 2015, **17**(37), 23963–23969.

17 R. Bhattacharjee, H. Jervis, M. E. McCormack, M. A. Petrukhina and M. Kertesz, Structure and Bonding in π-Stacked Perylenes: The Impact of Charge on Pancake Bonding, *J. Am. Chem. Soc.*, 2024, **146**(15), 10465–10477, DOI: **10.1021/jacs.3c14065**.

18 Z.-h. Cui, H. Lischka, H. Z. Beneberu and M. Kertesz, Double pancake bonds: Pushing the limits of strong π–π stacking interactions, *J. Am. Chem. Soc.*, 2014, **136**(37), 12958–12965.

19 L. Barluzzi, S. P. Ogilvie, A. B. Dalton, P. Kaden, R. Gericke, A. Mansikkamaki, S. R. Giblin and R. A. Layfield, Triply bonded pancake π-dimers stabilized by tetravalent actinides, *J. Am. Chem. Soc.*, 2024, **146**(6), 4234–4241.

20 M. E. McCormack, R. Bhattacharjee, H. Jervis, Z. Wei, M. Kertesz and M. A. Petrukhina, Stabilizing Cationic Perylene Dimers through Pancake Bonding and Equal Charge Share, *Cryst. Growth Des.*, 2023, **23**(10), 7496–7503, DOI: **10.1021/acs.cgd.3c00912**.

21 I. C. Lewis and L. Singer, Electron spin resonance of radical cations produced by the oxidation of aromatic hydrocarbons with SbCl$_5$, *J. Chem. Phys.*, 1965, **43**(8), 2712–2727.

22 J. L. Courtneidge, A. G. Davies and D. C. Mcguchan, The electron spin resonance spectra of the radical cations of *p*-terphenyl, triphenylene and triptycene, *Recl. Trav. Chim. Pays-Bas*, 1988, **107**(3), 190–196.

23 C. Kröhnke, V. Enkelmann and G. Wegner, Radical Cation Salts of Simple Arenes—A New Family of "Organic Metals", *Angew. Chem., Int. Ed. Engl.*, 1980, **19**(11), 912–919.

24 A. Kira and M. Imamura, Absorption spectra of dimer cations and other cationic species produced by warming of. gamma.-irradiated glassy solutions of aromatic hydrocarbons, *J. Phys. Chem.*, 1979, **83**(17), 2267–2273.

25 V. Kofman, P. Sarre, R. Hibbins, I. Ten Kate and H. Linnartz, Laboratory spectroscopy and astronomical significance of the fully-benzenoid PAH triphenylene and its cation, *Mol. Astrophys.*, 2017, **7**, 19–26.

26 Z. Zhou, O. Ungor, Z. Wei, M. Shatruk, A. Tsybizova, R. Gershoni-Poranne and M. A. Petrukhina, Tuning magnetic interactions between triphenylene radicals by

variation of crystal packing in structures with alkali metal counterions, *Inorg. Chem.*, 2021, **60**(19), 14844–14853.

27 M. Gorlov, A. Fischer and L. Kloo, One-step synthesis of a platinum (0)-gallium(III) chrysene complex, *Angew. Chem., Int. Ed.*, 2005, **44**(25), 3906–3908.

28 D. Freudenmann and C. Feldmann, $[Bi_3GaS_5]_2[Ga_3Cl_{10}]_2[GaCl_4]_2 \cdot S_8$ containing heterocubane-type $[Bi_3GaS_5]^{2+}$, star-shaped $[Ga_3Cl_{10}]^-$, monomeric $[GaCl_4]^-$ and crown-like S_8, *Dalton Trans.*, 2011, **40**(2), 452–456.

29 R. S. Mulliken and W. B. Person, *Molecular complexes: a lecture and reprint volume*, 1969.

30 Z. Mou, K. Uchida, T. Kubo and M. Kertesz, Evidence of σ- and π-Dimerization in a Series of Phenalenyls, *J. Am. Chem. Soc.*, 2014, **136**(52), 18009–18022.

31 J. P. Foster and F. Weinhold, Natural hybrid orbitals, *J. Am. Chem. Soc.*, 1980, **102**(24), 7211–7218.

32 F. L. Hirshfeld, Bonded-atom fragments for describing molecular charge densities, *Theor. Chim. Acta*, 1977, **44**, 129–138.

33 M. Rusyniak, Y. Ibrahim, E. Alsharaeh, M. Meot-Ner and M. S. El-Shall, Mass-selected ion mobility studies of the isomerization of the benzene radical cation and binding energy of the benzene dimer cation. Separation of isomeric ions by dimer formation, *J. Phys. Chem. A*, 2003, **107**(38), 7656–7666.

34 Z. Mou, Y.-H. Tian and M. Kertesz, Validation of density functionals for pancake-bonded π-dimers; dispersion is not enough, *Phys. Chem. Chem. Phys.*, 2017, **19**(36), 24761–24768.

35 I. K. Attah, S. P. Platt, M. Meot-Ner, M. S. El-Shall, R. Peverati and M. Head-Gordon, What is the structure of the naphthalene–benzene heterodimer radical cation? Binding energy, charge delocalization, and unexpected charge-transfer interaction in stacked dimer and trimer radical cations, *J. Phys. Chem. Lett.*, 2015, **6**(7), 1111–1118.

36 T. J. Kistenmacher, T. E. Phillips and D. O. Cowan, The crystal structure of the 1:1 radical cation–radical anion salt of 2,2′-bis-l,3-dithiole (TTF) and 7,7,8,8-tetracyanoquinodimethane (TCNQ), *Acta Crystallogr.*, 1974, **30**(3), 763–768.

37 J. Poater, M. Duran and M. Solà, Aromaticity determines the relative stability of kinked *vs.* straight topologies in polycyclic aromatic hydrocarbons, *Front. Chem.*, 2018, **6**, 425890.

38 T. Keszthelyi, G. Balakrishnan, R. Wilbrandt, W. A. Yee and F. Negri, Evidence of Dynamical Jahn–Teller Effect on Triphenylene Radical Cation: Resonance Raman Spectrum and *ab Initio* Quantum-Chemical Calculations, *J. Phys. Chem. A*, 2000, **104**(40), 9121–9129.

39 T. M. Krygowski, Crystallographic studies of inter-and intramolecular interactions reflected in aromatic character of. pi.-electron systems, *J. Chem. Inf. Comput. Sci.*, 1993, **33**(1), 70–78.

40 T. M. Krygowski and H. Szatylowicz, Aromaticity: what does it mean?, *ChemTexts*, 2015, **1**, 1–10.

41 E. Clar and R. Schoental, *Polycyclic hydrocarbons*, Springer, 1964.

42 Y. L. Zhang, M. Siskin, M. R. Gray, C. C. Walters and R. P. Rodgers, Mechanisms of Asphaltene Aggregation: Puzzles and a New Hypothesis, *Energy Fuels*, 2020, **34**(8), 9094–9107, DOI: 10.1021/acs.energyfuels.0c01564.

43 A. Frontera, D. Quiñonero, C. Garau, A. Costa, P. Ballester and P. M. Deyà, MP2 Study of Cation–$(\pi)_n$–π Interactions $(n = 1$–4$)$, *J. Phys. Chem. A*, 2006, **110**(30), 9307–9309.